Submitted to

International Europhysics Conference on High Energy Physics, EPS03, July 17-23, 2003, Aachen
(Abstract **091** Parallel Session **5**)

XXI International Symposium on Lepton and Photon Interactions, LP03, August 11-16, 2003, Fermilab

www-h1.desy.de/h1/www/publications/conf/conf_list.html

Diffractive dissociation in photoproduction at HERA

H1 Collaboration

Abstract

A new measurement of the differential cross section $d\sigma/dM_X^2$ for the process $\gamma p \to XY$, with a large rapidity gap between the systems X and Y and with Y a proton or a low mass proton excitation, is presented at three centre-of-mass energies $\langle W \rangle$ = 91,187 and 231 GeV. The trajectory intercept $\alpha_{eff}(0)$ obtained from a Regge parameterization of the W dependence with a single effective trajectory is presented as a function of M_X^2. A combined Triple Regge fit is performed over this rapidity gap data, in combination with leading proton data and fixed target data. The pomeron intercept $\alpha_{I\!P}(0)$ is extracted from this fit.

1 Introduction

At the HERA electron-proton collider, the bulk of the cross section corresponds to photoproduction, in which the electron is scattered through a very small angle and a quasi-real photon interacts with the proton. These photon proton interactions at high energies exhibit very similar properties to hadron interactions which can be understood as a photon fluctuating into a hadronic state [1] prior to the interaction with the proton. At high energies, hadron-hadron elastic and total cross sections have been successfully described in terms of the Regge picture in which two trajectories exchanged in the t-channel, the pomeron ($I\!P$) and the "reggeon" ($I\!R$), are important. At asymptotically large energies pomeron exchange dominates the elastic channel, resulting in a slow rise of the elastic and total cross section with energy. Processes in which one or both hadrons dissociate also occur (see Fig. 1) and are characterized by a large rapidity interval in which no hadronic activity is observed. These diffractive events dominate at large centre of mass energy and have small dissociative masses. The inclusive photon dissociative mass distribution can be modelled by combining Regge theory [2] with Mueller's generalization of the optical theorem [3], the so-called 'triple-Regge' approach.

Experimental results on diffractive dissociation processes have been studied at fixed target experiments [4], in pp and $\bar{p}p$ collisions [5, 6] and at HERA [7, 8]. At sufficiently high energies the diffractive dissociation process is dominated by the triple pomeron amplitude $I\!P I\!P I\!P$, leading to the differential cross section behavior $d\sigma/dM_X^2 \sim 1/M_X^2$. It was shown that for a better description of the data additional terms $I\!P I\!P I\!R$ [7, 8] and $I\!R I\!R I\!R$ [8] were required. The latter results [8] were obtained from a triple Regge analysis combining HERA data with fixed target measurements [4].

In the present paper, H1 data are presented from measurements of large rapidity gap events at three different W values $\langle W_{\gamma p} \rangle = 231, 187$ and 91 GeV, the latter data becoming available because of the installation of a new small angle electron tagger (eTag44) at 44 m. The data are interpreted in terms of a simple Regge approach to the W dependence at fixed M_X and also in the framework of a full triple Regge fit. To get better constraints on the triple-Regge fit parameters, leading proton data [9] providing a large range in M_X^2 and fixed target data [4] providing a larger lever-arm in W, were used in a simultaneous triple Regge fit.

2 Event selection

The data for this measurement were taken during a short dedicated run in 1997 in which HERA was colliding 27.5 GeV positrons with 820 GeV protons. An integrated luminosity of 2 pb^{-1} was collected. The events were triggered by a minimal total energy deposit from the hadrons in the backward SPACAL calorimeter in coincidence with a tagged electron in either the electron tagger at $z = -33$ m (eTag33) or in the tagger at $z = -44$ m (eTag44). Both of these taggers cover the range $Q^2 < 0.01$ GeV^2. Bremsstrahlung events ($ep \to ep\gamma$) were removed by requiring no energy above 2 GeV in the photon detector for the eTag33 data, and 0.6 GeV for the eTag44 data.

As the system Y was not tagged, the selection of single dissociative processes was based on an absence of significant activity in the forward detector system, comprising the Proton

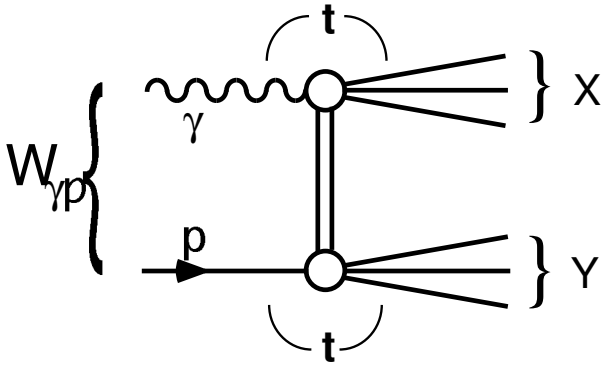

Figure 1: *Illustration of the generic process $\gamma p \to XY$. In the Regge pole picture, a reggeon is exchanged between the photon and the proton.*

Remnant Tagger (PRT), Forward Muon Detector (FMD) and the forward forward part of the Liquid Argon calorimeter (LAr):

- number of pre-toroid FMD paired hits < 3
- number of PRT scintillators giving a signal < 1
- no LAr clusters ($E >$ 400 MeV) at $\eta > 3.2$

With this selection, the pseudo-rapidity gap spans at least $3.2 < \eta < 7.0$.

Using Fig. 1 as the generic representation for a quasi two body process, in which there is a large rapidity gap between the X and Y systems, Y being closest to the proton beam direction, the events selected by the forward detectors correspond to the processes in which Y is either a proton or a low lying nucleon state with $M_Y < 1.6$ GeV. Furthermore the selection limits the square of the 4-momentum transfer from the incident proton to the system Y to $|t| < 1$ GeV^2. The sample also includes a fraction of non-diffractive events with an accidental gap in hadronic rapidity distribution due to a random fluctuation.

An important background in the data sample results from e^+ beam interactions with residual gas or the beam pipe wall, which have small values of $y = W^2/s$ reconstructed from hadrons (s is the square of the ep centre of mass energy). Most of this background in the eTag33 data sample was rejected by imposing the following cut:

$$y_{had} = \sum_{i=h} (E - P_z)_i / 2E_e > 0.2 \, ,$$

where the sum runs over all reconstructed hadrons. Using data from unpaired electron (pilot) bunches the remaining background is shown to be negligible. In the eTag44 data sample, corresponding to a smaller $W_{\gamma p}$, no such cut can be applied as the overlap between data and background is large. The background is subtracted statistically and is of the order of 10%.

3 M_X reconstruction

Having applied the forward detector selection, all particles observed in the central components of the detector are attributed to the system X. The mass of the system X is measured using the central components of the H1 detector. The M_X mass is reconstructed using an algorithm which combines particle track and calorimeter information whilst avoiding double counting. The invariant mass is then obtained using the expression:

$$M_X^2 = \left(\sum_{i\in X} E_i\right)^2 - \left(\sum_{i\in X} \vec{p_i}\right)^2 \simeq 2E_\gamma \sum_{i\in X} (E + P_z)_i \tag{1}$$

where i runs over all reconstructed objects of the system X and E_γ is the energy of the interacting photon, obtained from the measured scattered electron energy. This method has the advantage of being insensitive to the loss of very backward going hadrons ($E \simeq -P_z$).

4 Simulations

The PHOJET [10] and PYTHIA [11] Monte Carlo generators were used to correct for detector inefficiencies, acceptance corrections, trigger inefficiencies and smearing due to detector resolution. Both generators sub-divide diffractive photoproduction into the following processes:

- $\gamma p \to Vp$ (elastic case (EL));
- $\gamma p \to VY$ (single proton dissociation (PD));
- $\gamma p \to Xp$ (single photon dissociation (GD));
- $\gamma p \to XY$ (double dissociation (DD))

with $V = \rho,\ \omega,\ \phi$. Also non-diffractive events were simulated. At fixed W, the photon dissociative events are produced according to

$$\frac{d\sigma_{GD}}{dM_X^2 dt} \propto \frac{1}{M_X^2} e^{b_{GD}(M_X)t}$$

where b_{GD}, is the slope parameter for the GD process. Similar expressions exist for PD and DD [12]. The events are simulated in the region for which $M_X/W < 0.46$.

The generated mass distributions have been reweighted using an iterative procedure, until a satisfactory description of the reconstructed data is obtained.

5 Extraction of the differential cross section $d\sigma_{\gamma p}/dM_X^2$

From the eTag33 triggered data, two bins in W have been constructed. The first, $164 < W < 212$ GeV, yields a centre of mass energy averaged over the photon flux distribution of $\langle W \rangle$ = 187 GeV. The second range is $212 < W < 251$ GeV, corresponding to $\langle W \rangle$ = 231 GeV. For the eTag44 data an averaged centre of mass energy $\langle W \rangle$ = 91 GeV is obtained.

The differential cross section at $\langle W \rangle$ = 231 GeV, ($\langle W \rangle$ = 187 GeV) is measured in 7,(8) M_X^2 bins covering the range $4.00 < M_X^2 < 862$ GeV, (1860 GeV). For $\langle W \rangle$ = 91 GeV, measurements in the highest M_X region are no longer possible and the measured range is reduced to $1.58 < M_X^2 < 186$ GeV^2.

The PHOJET and PYTHIA Monte Carlos are used to correct the measured mass distribution for detector resolution and acceptance losses to a cross section defined in the kinematic range

$$M_Y < 1.6 \text{ GeV and } |\mathrm{t}| < 1 \text{ GeV}^2.$$

The mean acceptances of the electron taggers are 30 ± 2 % for the $\langle W \rangle = 231$ GeV sample, 45 ± 2 % for $\langle W \rangle = 187$ GeV and 34 ± 2% for $\langle W \rangle = 91$ GeV.

To obtain a γp cross section, the photon flux given by the Weizsäcker-Williams formula [13] has been used. Radiative corrections were found to be at the level of 1% in [14] and are neglected here.

The SPACAL trigger efficiencies for the $\langle W \rangle = 231$ and $\langle W \rangle = 187$ data have been cross checked using a data sample triggered on the basis of a vertex within 30 cm of the mean interaction point. The trigger efficiency was found to be almost 100% for all considered M_X bins. For the $\langle W \rangle = 91$ GeV data, the dissociating X-system is produced more forward such that the SPACAL trigger efficiency is reduced to about 40%. For all measured data points the stabilities and purities [1] are larger than 30%.

Statistical errors arise from the finite data volume, the samples used in the subtraction of the beam-gas background and the simulation samples used to make corrections. The statistical error in each interval is formed by adding the contributions from these three sources in quadrature. Systematic errors are evaluated on a bin by bin basis. The dominant source is the model dependence uncertainty in the acceptance corrections, evaluated from the difference between the results obtained when correcting with the PYTHIA and the PHOJET Monte Carlo models. The systematic errors and the statistical errors are then added in quadrature to give the total error.

The differential cross section measurement is shown in Fig. 2 and is compared for the two highest W-bins with the previous H1 measurement [8]. The results are consistent within the combined normalisation uncertainties.

[1] Purity (stability) is defined as the fraction of all simulated events reconstructed (generated) in a mass interval that are also generated (reconstructed) in that interval.

6 Results

6.1 Effective trajectory intercept as a function of M_X

The W dependence of the data is first tested at fixed M_X. Assuming a single effective trajectory of intercept $\alpha_{eff}(0)$ is exchanged, Regge theory predicts a centre of mass energy dependence for the cross section integrated over the t range of the measurement according to

$$\frac{d\sigma}{dM_X^2} \propto \left(W^2\right)^{2\alpha_{eff}(0)-2} \; \frac{e^{-B|t_{min}|} - e^{-B}}{B} \tag{2}$$

where $|t_{min}|$ is the minimum kinematically accessible vale of $|t|$ and B is the M_X dependent slope parameter.

Fitting the rapidity gap data to (2), with B constrained by fixed target data [8], the value of α_{eff} as a function of M_X^2 can be extracted. Fig. 3 shows the quality of the fits for the 6 M_X^2 bins considered. Fig. 4 shows the variation of $\alpha_{eff}(0)$ as a function of M_X^2. To the figure is also added the value of $\alpha_{eff}(0)$ obtained from fits using slightly different assumptions to H1 data in which the leading proton is tagged [9] in which higher M_X^2 values are reached. Fig. 4 shows that up to M_X^2 values of 300 GeV the cross section is dominated by the pomeron exchange ($\alpha_{eff}(0) \sim 1$). In the leading proton data subleading exchanges ($\alpha_R(0)$=0.5 and $\alpha_\pi(0)$=0.0) start to contribute, resulting in a lower value of the effective intercept. The extraction of the pomeron intercept from the triple Regge fit (section 6.2) is given by the band.

6.2 Triple Regge model

The differential cross section, $M_X^2 d\sigma/dM_X^2$ is shown in Fig. 6 together with a fit using a triple Regge model (see Fig. 5) performed on the presented cross section as well as on the cross sections from the leading proton data [9] and fixed target data [4]. In this model the cross section is expressed as a sum of contributions with reggeons i,j and k [15–18]:

$$\frac{d^2\sigma}{dM_X^2\, dt} = \frac{s_0}{W^4} \sum_{i,j,k} G_{ijk}(t) \left(\frac{W^2}{M_X^2}\right)^{\alpha_i(t)+\alpha_j(t)} \left(\frac{M_X^2}{s_0}\right)^{\alpha_k(0)} \cos\left[\phi_i(t) - \phi_j(t)\right]. \tag{3}$$

The trajectories $\alpha_i(t)$ are assumed to take the linear form $\alpha_i(t) = \alpha_i(0) + \alpha_i' t$. The functions $G_{ijk}(t)$ contain the products of all couplings. For photoproduction, the reggeons i and j must have the same signature such that $\phi_i(t) - \phi_j(t) = \frac{\pi}{2}\left[\alpha_j(t) - \alpha_i(t)\right]$.

The functions $G_{ijk}(t)$ and $\alpha_{ijk}(t)$ are not predicted by the model and must be determined from experimental measurements. The form (3) is fitted to the data with the six triple Regge couplings ($G_{I\!P I\!P I\!P}(0)$, $G_{I\!P I\!P I\!R}(0)$, $G_{I\!R I\!R I\!P}(0)$, $G_{I\!R I\!R I\!R}(0)$, $G_{\pi\pi I\!P}(0)$, $G_{\pi\pi I\!R}(0)$) and $\alpha_{I\!P}(0)$ as free parameters. The trajectories of the sub-leading exchanges and all t dependences are obtained from previous soft hadronic data. A factor of 3 is applied to the coupling for the isospin 1 π exchange in the rapidity gap data compared with the leading proton data, accounting for the additional possibility of leading neutron production and corresponding to the appropriate

Clebsch-Gordon coefficient. Since the exchange degenerate $I\!R$ trajectory contains both isospin 1 and isospin 0 exchanges, an additional free parameter $\mathcal{R}$ is introduced to multiply the $I\!R$ exchange couplings in the rapidity gap data. Interference terms ($i \neq j$) are not considered in the fit.

Fig. 6 shows the result of the fit for the different W-bins as well as the contributions of diffractive ($I\!P I\!P I\!P$ and $I\!P I\!P I\!R$), non-diffractive ($I\!R I\!R I\!P$ and $I\!R I\!R I\!R$) and pion terms ($\pi\pi I\!P$ and $\pi\pi I\!R$). From Fig. 6 it can be seen that a significant non-diffractive contribution is needed to explain the H1 rapidity gap data at large M_X. The fit yields the result $\mathcal{R} = 11.4 \pm 0.2\,(\mathrm{stat}) \pm 6.8\,(\mathrm{syst})$, significantly larger than the maximum expected value of 3. This suggests that a more complex treatment of the sub-leading exchanges is required for a complete description, probably including consideration of interference terms or the production of other baryon resonances in the rapidity gap data. However, the value obtained for $\alpha_{I\!P}(0) = 1.127 \pm 0.004\,(\mathrm{stat}) \pm 0.025\,(\mathrm{syst}) \pm 0.046(\mathrm{model})$ is stable with respect to different assumptions concerning the sub-leading exchanges. The new measurement of $\alpha_{I\!P}(0)$ is shown in Fig. 7 together with previous measurements as a function of Q^2. An indication of a rising pomeron intercept is seen as a function of Q^2.

7 Conclusion

The differential cross section $M_X^2\ d\sigma_{\gamma p \to XY}/dM_X^2$ for $M_Y < 1.6$ GeV and $|t| < 1.0$ GeV^2 has been measured for photoproduction data at HERA. The precision is improved at $W \sim 200$ GeV and measurements are made for the first time at $W \sim 100$ GeV. From the W dependence of the data, the intercept $\alpha_{eff}(0)$ of an *effective* trajectory as a function of M_X^2 is determined. It is found that at small M_X^2 values up to 300 GeV, the pomeron trajectory dominates. The data are also subjected to a triple Regge decomposition, in which the M_X and W dependences are simultaneously described. The resulting pomeron trajectory intercept is consistent with the result for the soft pomeron describing other soft hadronic cross sections.

References

[1] J. Sakurai, Ann. Phys. **11** (1960) 1
D. Yennie, Rev. Mod. Phys. **47** (1975) 311

[2] P. Collins, *An introduction to Regge theory and high energy physics*

[3] A. Mueller, Phys. Rev. **D2** (1970) 2963

[4] T. Chapin et al., Phys. Rev. **D31** (1985) 17

[5] E-710 Collaboration, N. Amos et al., Phys. Lett. **B301** (1993) 313

[6] CDF Collaboration, F. Abe et al., Phys. Rev. **D50** (1994) 5535

[7] ZEUS Collaboration, Zeit. Phys. **C75** (1997) 421

[8] H1 Collaboration, J. Adloff et al., Zeit. Phys. **C74** (1997) 221

[9] H1 Collaboration, J. Adloff et al., Nucl. Phys. **B619** (2001) 3

[10] R. Engel, Zeit. Phys. **C66** (1995) 203
R. Engel, J. Ranft, Phys. Rev. **D54** (1996) 4244

[11] H. Bengtsson, T. Sjöstrand, Comp. Phys. Commun. **46** (1987) 43
H. Bengtsson, T. Sjöstrand, Comp. Phys. Commun. **82** (1994) 74

[12] P. Newman, *A study of the Dynamics of Diffractive Photoproduction at HERA.*, Ph.D thesis (University of Birmingham) 1996.

[13] C. Weizsäcker, Z. Phys. **88** (1934) 612
E. Williams, Phys. Rev. **45** (1934) 729
S. Frixione et al., Phys. Lett. **B319** (1993) 339

[14] H1 Collaboration, S. Aid et al., Zeit. Phys. **C69** (1995) 27

[15] A. Kaidalov, Phys. Rep. **50** (1979) 157

[16] G. Alberi, G. Goggi, Phys. Rep. **74** (1981) 1

[17] K. Goulianos, Phys. Rep. **101** (1983) 169

[18] N. Zotov, V. Tsarev, Sov. Phys. Usp. **31** (1988) 119

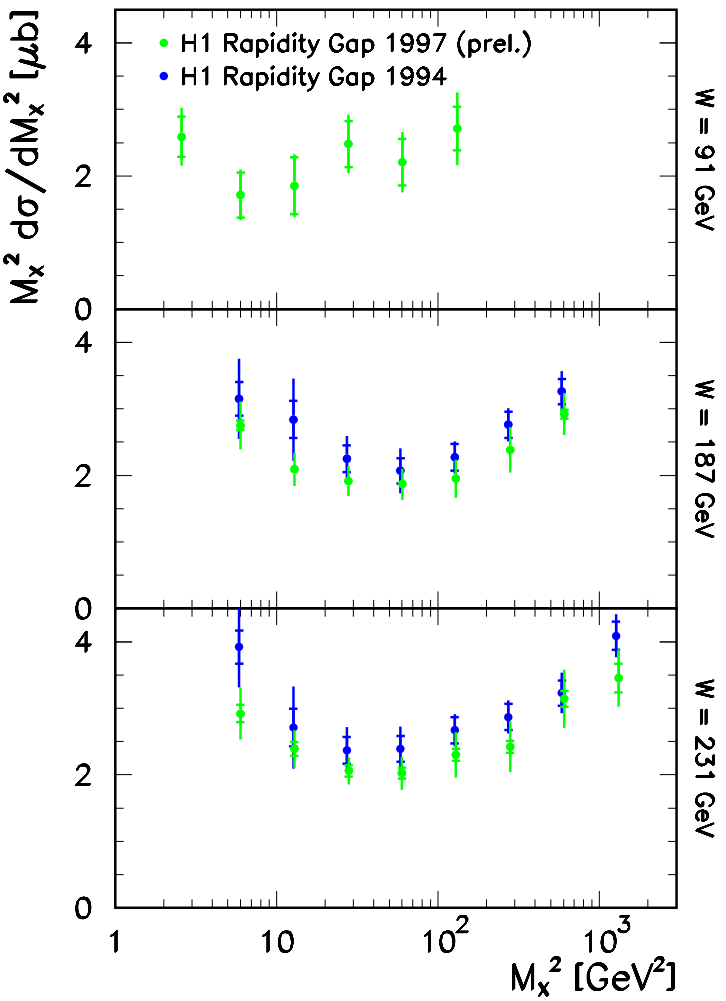

Figure 2: *The Differential cross section measurement* $M_X^2 \; d\sigma/dM_X^2$ *for* $M_Y < 1.6$ *GeV and* $\mid t \mid < 1$ *GeV*^{2}*. A comaprison with a previous H1 measurement is made for the* γp *center of mass energies* W*=231 and 187 GeV. The new measurement yields additional data at* W*=91 GeV.*

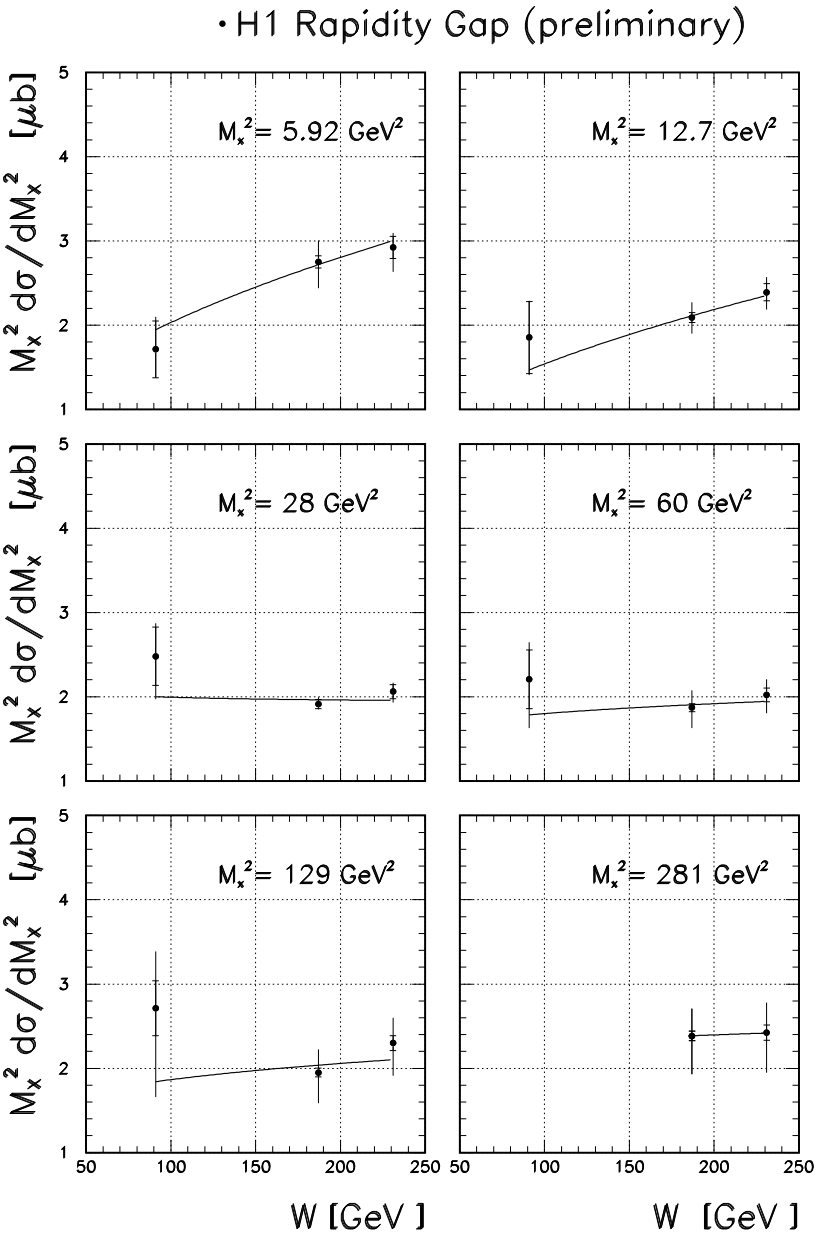

Figure 3: For each fixed M_x^2-bin measured, the W dependence is fitted to extract an effective intercept $\alpha_{eff}(0)$. The results of the fits are shown for each M_x^2-bin.

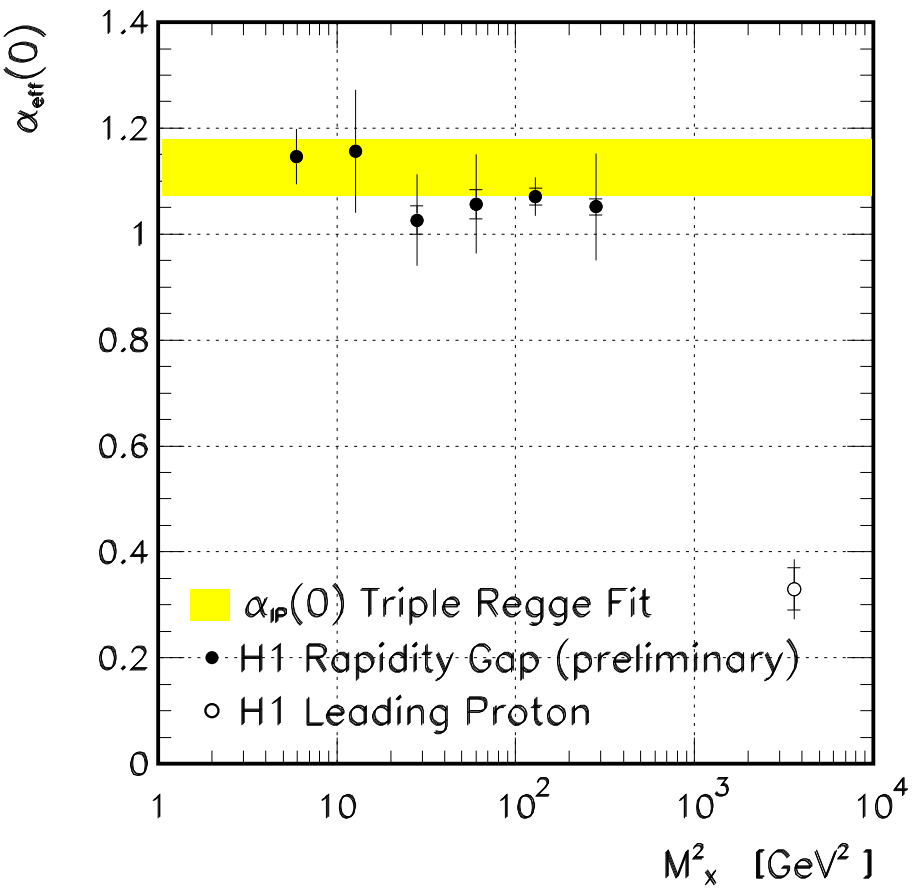

Figure 4: The M_x^2 evolution of $\alpha_{eff}(0)$ is shown from H1 data. One additional point is added from the leading proton data [9]. For comparison, the shaded band shows the result for $\alpha_{I\!P}(0)$ from the triple Regge fit, where the M_X dependence is also fitted.

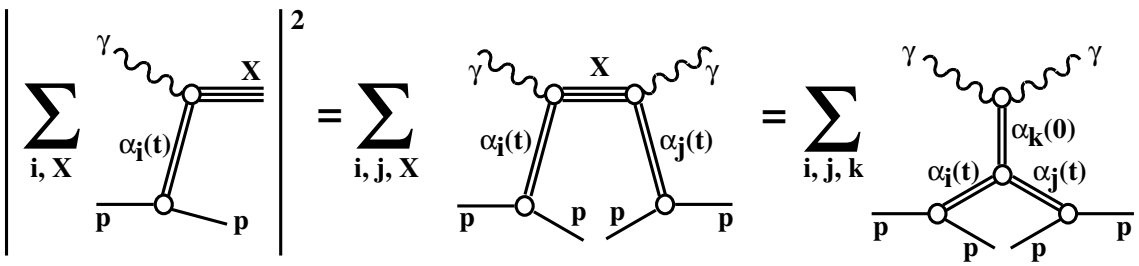

Figure 5: *Illustration of the Mueller-Regge approach to the inclusive photon dissociation cross section. It relates the sum over all final states X to the forward amplitude for the process* $\gamma\ \alpha_i(t) \to \gamma\ \alpha_j(t)$ *at an effective centre of mass energy* M_X *(middle diagram). For sufficiently large* M_X*, a Regge expansion for the photon-reggeon scattering amplitude is also appropriate, such that the dissociation cross section may be decomposed into triple-Regge terms as shown in the last diagram of the figure.*

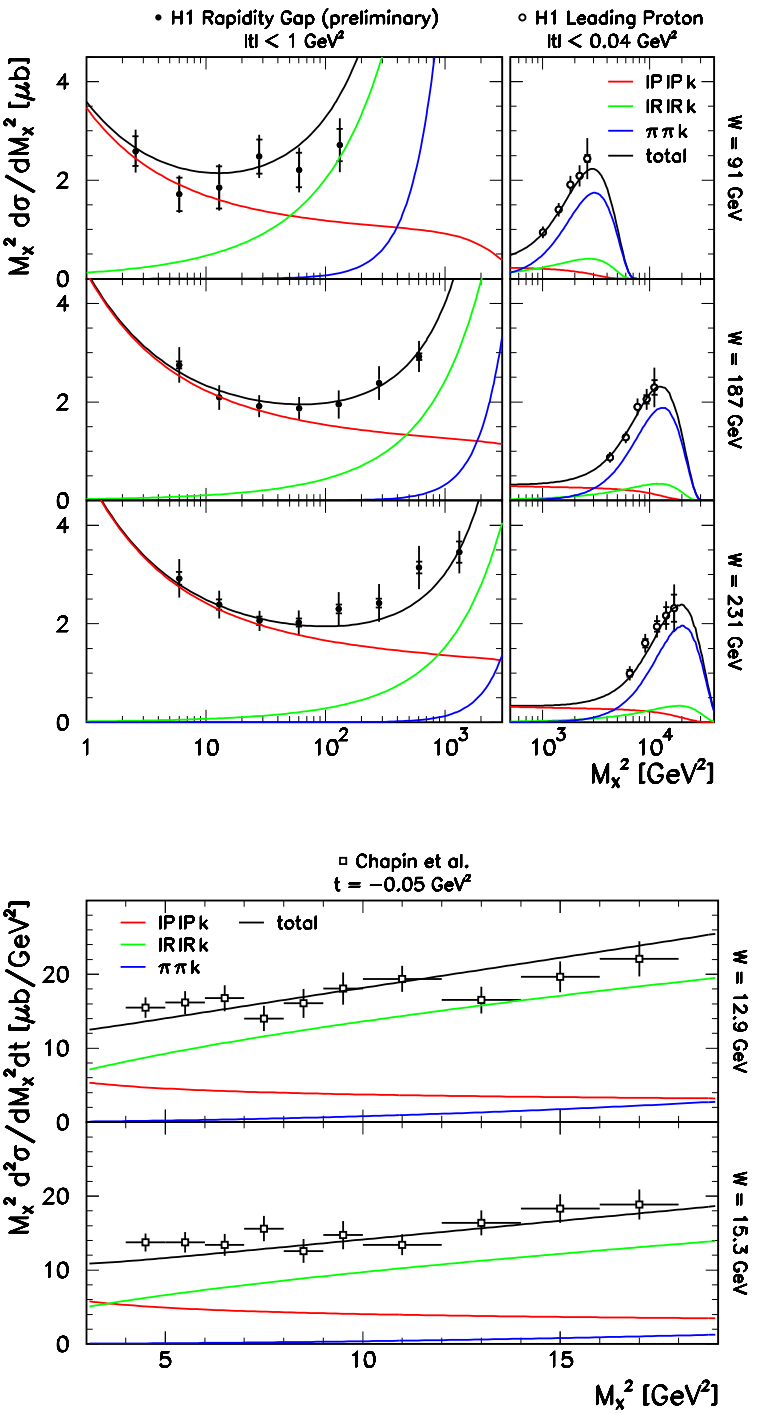

Figure 6: The results of the Triple Regge fit performed over the present H1 rapidity gap data, the H1 leading proton data [9] and fixed target data [4]. The details are explained in the text.

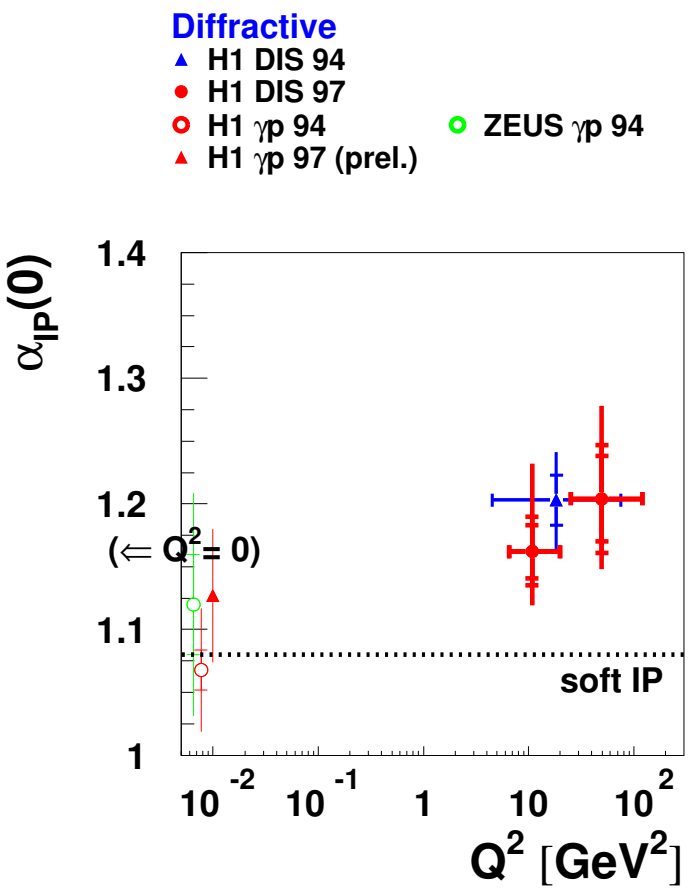

Figure 7: A summary of H1 $\alpha_{I\!P}(0)$ measurements versus Q^2 for $\gamma^{(*)}p \to Xp$. A previous ZEUS result [7] at $Q^2 = 0$ is also shown.